HOSTED BY

ELSEVIER

Available online at www.sciencedirect.com

ScienceDirect

Soils and Foundations 62 (2022) 101098

www.elsevier.com/locate/sandf

Technical Paper

A unified approach to link small-strain shear modulus and liquefaction resistance of pumiceous sand

Mohammad Bagher Asadi [a,*,1], Rolando P. Orense [b], Mohammad Sadeq Asadi [c], Michael J. Pender [b]

[a] Jacobs New Zealand Limited, Auckland 1010, New Zealand
[b] Dept. of Civil and Environmental Engineering, Univ. of Auckland, Auckland 1142, New Zealand
[c] Dept. of Civil Engineering, Shahid Bahonar Univ. of Kerman, Kerman 76169-14111, Iran

Received 18 May 2021; received in revised form 11 November 2021; accepted 12 December 2021

Abstract

Natural pumiceous (NP) sands containing pumice particles, a type of volcanic soil, are commonly found in the central part of the North Island in New Zealand. The pumice particles are highly crushable, compressible, lightweight and angular, making engineering assessment of their properties problematic. In this paper, several series of bender element and undrained cyclic triaxial tests were performed on reconstituted and undisturbed NP sands to determine their small-strain shear modulus (G_{max}) and cyclic resistance ratio (CRR). Furthermore, similar tests were also conducted on normal hard-grained sands (e.g., Toyoura sand) for the purpose of comparison. The results showed that the NP sands have considerably lower G_{max} compared to normal sands, resulting in their higher deformability during the initial stages of the cyclic loading test. The high angularity of NP sands play an important role toward the end of the cyclic loading and contributed to their higher CRR. Next, the ratio of CRR/G_{max} for each sample was correlated to a level of strain denoted as cyclic yield strain (ε_{ay}), which was found to be significantly dependent on the percentages of pumice particles present in the natural soils. On the other hand, the ε_{ay} was found to be less sensitive to the consolidation stress (σ'_c) and the relative density (Dr) of the materials. For example, over different values of σ'_c and Dr, NP sands have substantially higher values of cyclic yield strain due to their lower G_{max} and higher CRR when compared with those of ordinary sands.

Keywords: Pumiceous sand; Particle crushing; Liquefaction resistance; Small-strain shear modulus; Volcanic soils

1. Introduction

Liquefaction occurrence in loose and saturated sands is due to their contractive tendency (in volume) during earthquake shaking. This tendency during cyclic loading leads to the transformation of normal stress between soils grains onto pore water pressure. Then, the reduction in effective confining stress within the soil assembly results in a significant loss of strength that contributes to soil deformation (Idriss and Boulanger, 2008). The volume change of sands during cyclic loading is known to be more uniquely related to the shear strain imposed onto the soil deposit rather than to the applied shear stress (Dobry et al., 2015; Seed et al., 1983). Extensive experimental investigations in the literature pointed out that normal sands have a similar volumetric cyclic threshold shear strain (γ_{tv}), which corresponds to a level of strain where saturated sand starts to build up pore water pressure under undrained cyclic load-

Peer review under responsibility of The Japanese Geotechnical Society.
* Corresponding author.
E-mail addresses: masa093@aucklanduni.ac.nz (M.B. Asadi), r.orense@auckland.ac.nz (R.P. Orense), m.pender@auckland.ac.nz (M.J. Pender).
[1] Formerly University of Auckland.

https://doi.org/10.1016/j.sandf.2021.101098
0038-0806/

ing (Abdoun et al., 2013; Dobry et al., 1982; Hsu and Vucetic, 2004). Thus, the γ_{tv} is an important geotechnical parameter, which provides a boundary to separate two different cyclic behaviours, i.e. the matrix of soil grains is kept intact when the applied cyclic shear strain (γ_c) is lower than γ_{tv} (no pore water pressure generated); however, the structure of soil particles would deform once $\gamma_c > \gamma_{tv}$ with observation of pore water pressure build-up (Hsu and Vucetic, 2004). The above findings indicate the predictive power of the strain-based parameters in estimating pore water pressure generation, and consequently in liquefaction assessment of sands. Note that the normal sands referred to in this paper are hard-grained quartz-type sands that do not crush under moderate practical pressures.

Investigations using strain-based approaches indicate the existence of a unique constant cyclic shear strain needed for liquefaction (i.e. γ_{cl}) that can be utilised to provide boundaries between liquefiable and non-liquefiable sands (Dobry et al., 2015). The existence of this γ_{cl} was observed in the lower end of liquefaction assessment charts based on simplified procedures, such as cone penetration test (CPT), standard penetration test (SPT) and shear wave velocity (V_s) methods (Andrus and Stokoe, 2000; Dobry, 1989; Seed et al., 1983). In addition, Amoly et al. (2016) proposed the cyclic yield strain (ε_{ay}) concept using stress-controlled undrained cyclic triaxial tests. The ε_{ay} parameter is a threshold axial strain, which corresponds to the beginning of the occurrence of large deformation in the specimen; whereas, γ_{tv} is a threshold shear strain marking the start of pore water pressure build-up. The average value of γ_{tv} obtained for different quartz-type sands is around 0.01% (Hsu and Vucetic, 2004), while the average range of ε_{ay} (for two types of Japanese sands) expressed in the form of shear strain, $\gamma_y = 1.5\ \varepsilon_{ay}$ (valid for undrained loading, per Ladd et al. (1989)), is about $\gamma_y = 1.5 \times (0.036–0.046\%) = 0.054–0.069\%$. In this range of ε_{ay}, the pore water pressure is noticeably increased during cyclic loading marking the ε_{ay} as a strain-level benchmark where high pore water pressure can be developed within the sample (Amoly et al., 2016). Consequently, the ε_{ay} was utilised as a strain parameter to develop boundaries between liquefiable and non-liquefiable sands.

While Amoly et al. (2016) introduced the important advantages of using the concept of ε_{ay} in liquefaction assessment of normal sands, limited/no investigation was made on the sensitivity of ε_{ay} to relative density (D_r), confining pressures (σ'_c) and fines content (FC); these parameters can have significant effects on the liquefaction resistance of sands. Then, the effect of the above parameters on ε_{ay} is required to be investigated. Furthermore, it is important to investigate the applicability of such concept in the case of soft/crushable volcanic soil, which can be found in different locations around the world, such as Japan, Italy, Chile and New Zealand. Natural pumiceous (NP) sands, a type of volcanic soils, exist in many locations in the central part of North Island in New Zealand. The pumice particles present in the NP sands originated from a series of volcanic eruptions in the Taupo Volcanic Zone. Powerful eruptions and airborne transport resulted in air fall deposits. These deposits were subsequently eroded and the material transported in a fluvial environment and mixed with other materials, such as ordinary and/or fine materials before deposition (McCraw, 2011). Pumice sands are characterised by a number of distinctive properties such as crushability, compressibility and lightweight features (Orense et al., 2012). In addition, the existence of many surface voids in pumice particles leads to their irregular surface texture, which enables them to have higher angle of internal friction (Kikkawa et al., 2013). The irregular shape of pumice particles is compared with normal sand particles in Fig. 1 using scanning electron microscopic (SEM) images.

In this paper, to investigate the cyclic yield strain (ε_{ay}) of crushable NP sands, several series of bender element (BE) tests and stress-controlled undrained cyclic triaxial tests were performed on reconstituted and undisturbed NP specimens. For comparison purposes, similar laboratory tests were also performed on normal sands. First, the sensitivity of ε_{ay} to confining pressure (σ'_c) and relative density (D_r) was examined using reconstituted specimens. Next, the combined results from undisturbed and reconstituted specimens were used to understand the important effect of the crushable pumice components in the natural soils on their cyclic yield strain when compared with normal sands. The effect of FC and sample disturbance on ε_{ay} was also partially examined.

2. Field performance of volcanic soil to past earthquakes

One of the main concerns which will be addressed in this paper is the geotechnical characteristics of volcanic soils (including pumiceous sands) and their susceptibility to liquefaction. Volcanic soils are present in some parts of Japan (Hyodo et al., 1998; Miura et al., 2003; Sahaphol and Miura, 2005; Suzuki and Yamamoto, 2004), Italy (de Cristofaro et al., 2022; Papa et al., 2008; Picarelli et al., 2007), South/Central America (Crenairz, 2010; Sandoval and Pando, 2012) and New Zealand (Beanland et al., 1989; Orense et al., 2012). The Taupo Volcanic Zone (TVZ), in the central region of the North Island, New Zealand, has extensive deposits of volcanic ash and pumiceous sands. Following the 1987 Edgecumbe earthquake (M_w 6.3), localised liquefaction in the form of sand boils was observed in the northeast section of the TVZ (Pender and Robertson, 1987). This event revealed the high susceptibility of pumiceous sands to liquefaction under seismic loading (Marks et al., 1998).

Furthermore, several parts of Japan are covered by volcanic ash sediments due to Japan's tectonic location; some of these volcanic soils are known as Shirasu and pumice sands. Shirasu is mainly distributed in Southern Kyushu and is very crushable due to the brittleness of the particles, and the low particle density ($G_s = 2.4–2.5$) when compared to other hard-grained soils (Ishihara and Harada, 1994;

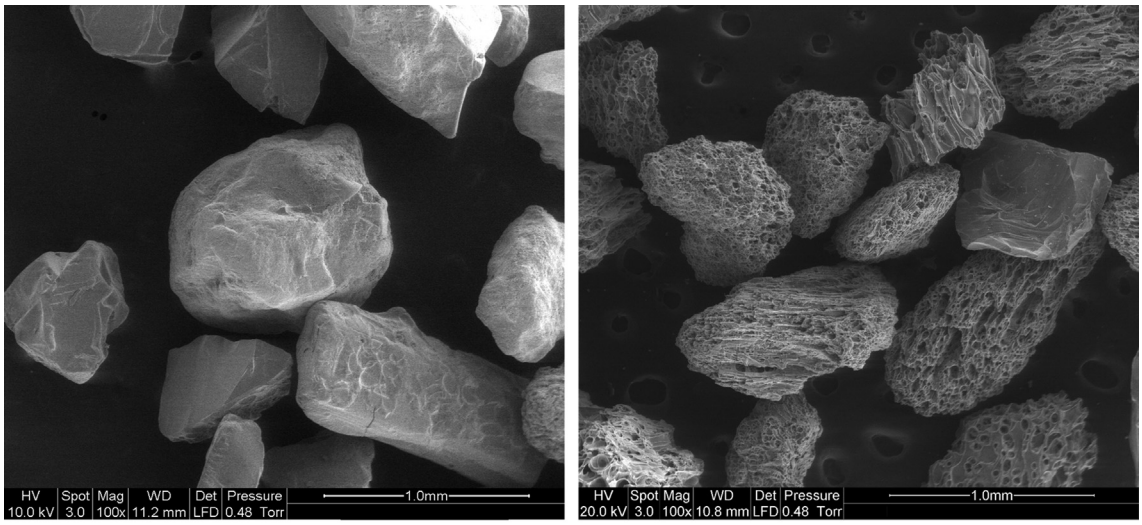

Fig. 1. Comparison of pumiceous sands with predominately (a) normal sand particles (from NP_{HMTR} site); and (b) pumice sand particles (from NP_{HMGS} site).

Suzuki and Yamamoto, 2004). In the two Ebino earthquakes (1968) and the Northwestern Kagoshimaken earthquake (1997), it was observed that Shirasu sands liquefied, and some damage to infrastructure was observed (Suzuki and Yamamoto, 2004). In terms of pumiceous soil behaviour during an earthquake, the Iwate-Miyagi Nairiku earthquake (2008) in Japan resulted in the largest landslide (i.e., the Aratozawa landslide) in pumiceous deposits (Gratchev and Towhata, 2010; Kazama et al., 2012). The Miyagi Nairiku earthquake (2008) triggered a landslide with a volume of about 1.5 million m^3 followed by mudflow that travelled approximately 10 km downstream (Kazama et al., 2012). Furthermore, the occurrence of liquefaction and landslides were observed in volcanic soil deposits during the M_w7.0 Kumamoto earthquake (2016) and the M_w6.6 Hokkaido earthquake (2018) (Hazarika et al., 2017; Kokusho et al., 2019). The presence of orange-coloured pumice particles was observed in the landslide material after the 2016 Kumamoto earthquake, and it is believed that the landslide was mobilised within these pumice sand layers (Hazarika et al., 2017). The above observations show that these volcanic soils are susceptible to liquefaction, highlighting the importance of conducting experimental investigations to characterise their liquefaction resistance.

3. Specimen preparation and materials used

In this paper, reconstituted and undisturbed specimens were prepared/obtained to investigate the dynamic properties of NP sands. Fig. 2 shows the locations where the NP sands were obtained in the North Island. The collected NP sands for reconstituted testing are denoted as NP1, NP2 and NP3 sands, while the undisturbed specimens are referred to as NP_{HMGS}, NP_{HMTR}, NP_{WH}, NP_{ED}, NP_{TA} and NP_{TA7} sands. As part of the research project, these sites were identified from existing borehole logs to contain layers with pumice sands. The sample preparation methods for (1) reconstituted, and (2) undisturbed specimens are explained as follows:

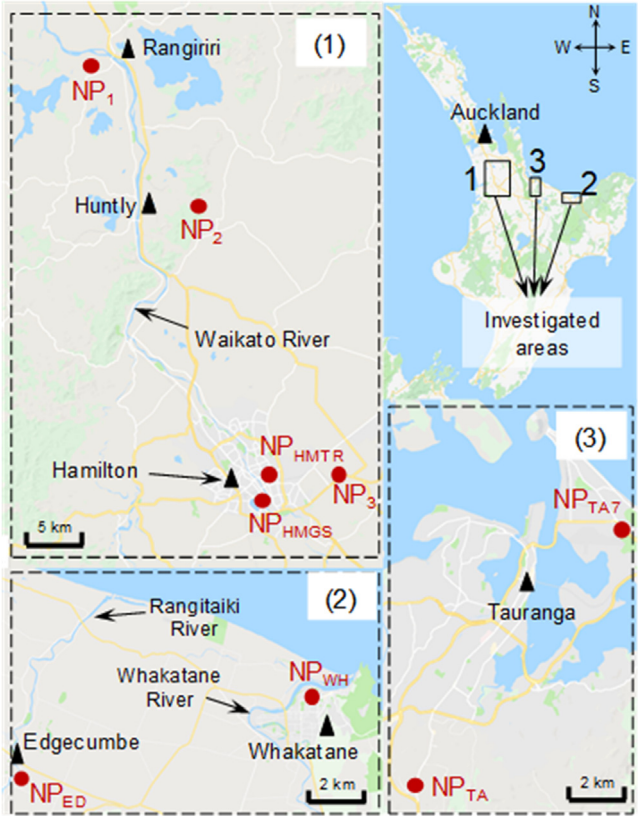

Fig. 2. Locations where pumiceous specimens were obtained (map from Google Earth).

(1) To produce uniform reconstituted specimens, the moist tamping method was followed to eliminate the segregation of lightweight pumice particles from non-pumice components in the NP sands. A split mould, with the size of 63 mm diameter and 126 mm height, interiorly covered by a membrane, was utilised in preparing the reconstituted samples. Then, a pre-weighed quantity of the sands based on a target initial relative density was compacted in five layers inside the mould until a certain thickness for each layer reached. Next, a groove for the BE was made on the top of the specimen, using a special cap with a slot for the BE, with the same size and orientation as the BE attached to the pedestal. Note that the piezoelectric BEs (coated with epoxy) attached to the pedestal and top cap were 21 mm long, 17 mm wide, 1.7 mm thick, and protruded 10 mm into the ends of the soil specimen. Care was needed to ensure that the protrusions were vertical. Also, the correct alignment of the two bender elements was necessary to ensure maximum energy transmission and to minimise near-field effects due to the boundary reflection of the signal.

(2) The undisturbed specimens were retrieved using two sampling techniques, i.e. gel-push triple tube (GP-TR) and Dames & Moore (DM) sampling; both samplers are hydraulically-activated fixed piston and Osterberg-type sampling devices (Stringer et al., 2015). In the case of gel-push sampling, a polymer gel lubricant was utilised during the drilling of the sampler into the ground to reduce the sidewall friction between the *PVC* (polyvinyl chloride) tube and the outside surfaces of the soil samples. The GP-TR tube sampler was 1000 mm in height and 83 mm in diameter. On the other hand, the DM sampler employed a thin-walled brass tube to retrieve the intact soil specimens; a brass tube was used due to its lower coefficient of friction with the soil specimens. The DM sampler tube was 450 mm in height and 61 mm in diameter. After obtaining the undisturbed specimens, the samples were drained vertically at the site and then frozen using dry ice in order to eliminate the possible disturbance to the specimens during transport. After transporting to the laboratory, the specimens were kept frozen during the whole process of sample preparation; however, the specimen surface was allowed to thaw a bit for trimming the specimens to the target size of 126 mm height and 63 mm diameter. Next, a three-part split mould was utilised to level both ends of the undisturbed specimen as well as to make the grooves (using a special cap with the slot of BE size) on top and bottom of the sample for the BE, with the same orientations using the special cap with the slot for the BE.

In the next stage, the specimens were saturated by increasing the cell-pressure and back-pressure in different stages for a period of 24 h to achieve a B-value > 0.95; the specimens were fully saturated when subjected to back-pressure of 600 kPa. It should be noted that the specimens were gradually saturated at different stages, and during each stage, the difference between the cell-pressure and the back-pressure was kept low at about 10 kPa. Based on experience, this process would result in practically no disturbance to the structure of the specimens even when subjected to such high level of back-pressure. In the next stage, the specimens were isotropically consolidated at different target effective confining pressures (σ'_c).

The index properties, e.g., specific gravity (G_s), maximum void ratio (e_{max}), minimum void ratio (e_{min}), and fines content (FC), of the NP sands used as well as those of Toyoura sand are shown in Table 1 while their particle size distribution (PSD) curves are shown Fig. 3. The Japanese standard method (JGS, 2000) and New Zealand standard method (NZS4402 (Standards New Zealand, 1986)) were followed to determine the maximum/minimum dry densities and specific gravity (G_s) of the tested materials, respectively. Note that the Japanese standard method was utilised to ensure that no particle crushing would occur during the maximum dry density test. Fig. 3 also depicted the PSD ranges of sands with the "possibility of liquefaction" and "high possibility of liquefaction" introduced by the Ministry of Transport Japan (1999). It is evident from Fig. 3 that most PSD curves of NP sands are within the range of sands identified to be of "high possibility of liquefaction". To determine the PSD curves of the samples, the New Zealand standard method (NZS4402 1986) was used to perform wet sieve tests. Due to the limited number of specimens available for undisturbed testing, it was not possible to perform the test on the fresh undisturbed samples; therefore, the materials after triaxial testing were used for the sieve tests. On the other hand, fresh materials were used for the sieve tests in the case of reconstituted samples. It should be noted that the extra materials from the trimming of the undisturbed specimens were not appropriate to use, as they underwent significant amount of particle crushing when the soil lathe was used to trim the periphery of the specimens. Therefore, while the PSD curves shown for the undisturbed samples may have been affected by some level of particle crushing, such would not significantly affect their general PSD curves.

It has been reported that the pumice particles present in the NP sands have a complex surface texture with many surface voids. The irregular shape of pumice sand grains can be seen in Fig. 1 (b). The methodology of Kikkawa et al. (2013), which was adopted by Asadi et al. (2018), was used to analyse the SEM images to quantify the soil particle shape characteristics through angular coefficient (A_c) and aspect ratio (A_r). Detailed calculation of A_c and A_r was reported by Asadi et al. (2018) where they observed that the particle shape characteristics of the investigated NP sand particles were approximately three times more angular (related to A_c) and 1.3 times more elongated (related to A_r) than Toyoura sand particles.

Table 1
Index properties of materials used.

Site	Sample ID	Depth (m)	No. tests	G_s	e_{max}	e_{min}	FC (%)	PC (%)	Range of e_c
NP_{HMGS}	GPTR1-4	6.5	6	2.30	3.02	1.89	68	93	2.32–2.51
NP_{HMGS}	GPTR1-5	7.9	4	2.33	3.01	1.88	45.2	93	2.08–2.36
NP_{HMGS}	DM1-2	2.7	2	2.40	0.86	0.61	1.5	35	0.78–0.80
NP_{HMTR}	GPTR2-2	3.0	4	2.61	0.90	0.60	0.5	18	0.67–0.71
NP_{HMTR}	DM1-6 & DM1-7	10.9	4	2.52	1.11	0.88	0.5	38	0.99 – 1.01
NP_{WH}	GPTR2-3	3.4	4	2.29	2.69	1.86	5.0	88	1.98–2.10
NP_{WH}	GPTR3-3	5.0	6	2.45	1.58	1.01	1.0	55	1.15–1.23
NP_{WH}	DM4-2	4.2	2	2.49	1.89	1.13	1.6	38	1.32–1.39
NP_{WH}	GPS1-1	0.9	4	2.37	2.21	1.43	5.0	71	1.71 – 1.78
NP_{WH}	GPS1-3	2.2	3	2.57	1.42	0.80	8.0	30	0.99 – 1.05
NP_{WH}	GPS3-1	3.65	4	2.53	0.99	0.78	0.5	–	0.82–0.84
NP_{ED}	GPTR1-1	2.9	4	2.59	1.28	0.79	5.0	25	–
NP_{ED}	GPTR1-2	4.0	6	2.50	1.03	0.67	0.5	36	0.77–0.80
NP_{ED}	GPTR1-4	5.5	5	2.48	1.00	0.75	0.5	39	0.82 – 0.84
NP_{ED}	GPTR2-2	4.0	4	2.49	1.14	0.86	0.5	42	0.93 – 0.95
NP_{ED}	GPTR2-3	5.5	5	2.26	1.26	1.02	0.5	62	1.09–1.11
NP_{TA}	DM1-3 & DM1-4	7.5	6	2.57	1.33	0.73	12.0	19	1.07 – 1.12
NP_{TA}	DM1-1 & DM1-2	4.0	6	2.35	3.21	2.09	36.4	72	2.22 – 2.31
NP_{TA}	DM2-1	3.2	3	2.44	1.84	1.31	14.0	–	1.44–1.46
NP_{TA7}	GPTR1-1	2.7	3	2.66	0.99	0.66	0.5	0	0.72–0.74
NP_{TA7}	GPTR1-2	4.9	3	2.45	1.67	1.19	2.5	45	1.28–1.30
NP_{TA7}	GPTR1-3	6.7	3	2.47	1.62	1.15	0.8	43	1.23–1.25
NP1	Reconstituted	4.5	10	2.54	1.74	1.04	12.3	39	1.18–1.53
NP2	Reconstituted	5.95	11	2.48	1.56	0.95	16.7	49	1.07–1.38
NP3	Reconstituted	1.5	9	2.53	0.99	0.65	2.5	21	0.72–0.89
Toyoura	Reconstituted	–	8	2.66	0.89	0.61	0	0	0.67–0.75

The NP sands collected from different sites also have different pumice contents, defined as the proportion of pumice particles by weight in a soil matrix. To estimate the pumice content (PC) of the different NP sands, the methodology proposed by Asadi et al. (2019) was followed. According to this approach, the PC of the NP specimens was estimated based on the level of particle crushing occurrence during a modified maximum dry density (MDD) test. The amount of particle crushing was quantified through the relative breakage (Hardin, 1985) using the PSD curves before and after the MDD test. Relative breakage, B_r, is the ratio of the total breakage, B_t (i.e., enclosed area between the PSD curves before and after testing) to the potential breakage, B_p (i.e., the enclosed area between the initial PSD curve and upper limit for silt size, i.e., 0.063 mm). Then, the PC of NP sands was estimated using the PC- B_r relation proposed by Asadi et al. (2019) and these are shown in Table 1.

4. Laboratory tests

To measure the shear wave velocity (V_s) of the reconstituted and undisturbed NP specimens, bender element (BE) tests were first performed on the consolidated specimens at different σ'_c. The V_s was calculated using the equation, $V_s = d/t$, where d the is the tip-to-tip distance between the bender elements, while t is the shear wave travel time between the bender elements (Shirley and Hampton, 1978); peak-to-peak arrival time method was used to calculate t. Then, the calculated values of V_s were converted to the small-strain shear modulus (G_{max}) using the equation, $G_{max} = \rho V_s^2$, where ρ is the bulk density of the soil specimens. The values of ρ were estimated according to the sample's void ratio after consolidation (e_c) following the Verdugo and Ishihara (1996) approach; the range of e_c values measured from the sample tested are reported in Table 1.

Regarding the accuracy of BE test results, the comprehensive study of Yang and Gu (2013) showed that the G_{max} values obtained from BE test are comparable with those measured using other methods, such as by the resonant column device, with just ±10% variation. This minor difference between the two methods may be due to the different strain levels used for G_{max} measurements in both BE and resonant column tests (Yang and Gu, 2013). Furthermore, the BE test results showed that the G_{max} values are considerably dependent on the physical states of the soil samples, e.g., relative density and confining pressure. Using the reconstituted test results shown in Fig. 4, the G_{max} values of the tested samples are highly dependent on the relative density and confining pressure of samples. i.e., as the magnitudes of relative density and confining pressure increase, their G_{max} also tend to increase (see Asadi et al. (2020) for more details on the response of G_{max} of NP sands under variable states).

After the BE tests, the specimens were subjected to sinusoidal cyclic loading with a frequency of 0.1 Hz under stress-controlled and undrained conditions. Different levels of cyclic stress ratio (CSR) were applied to the specimens until a deformation greater than 5% double amplitude axial

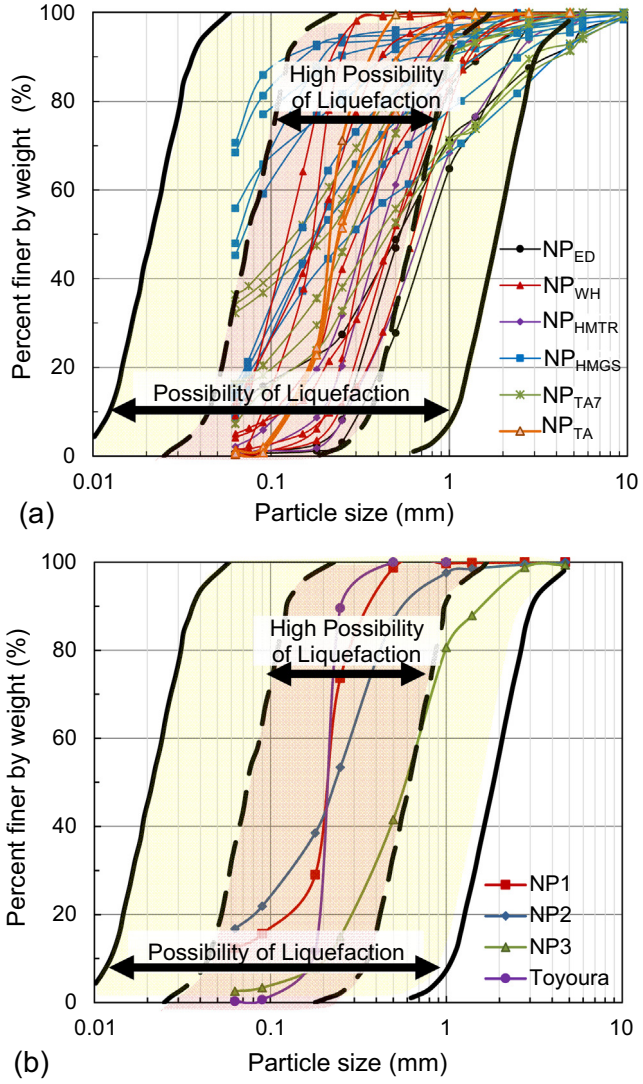

Fig. 3. Particle size distribution curves of (a) undisturbed; and (b) reconstituted samples.

strain (ε_{DA}) was observed. Here, $CSR = q/2\sigma'_c$, where q is the deviator stress and quantified as the difference between the effective axial stress (σ'_1) and effective lateral stress (σ'_c), i.e., $q = \sigma'_1 - \sigma'_c$. The mean effective stress is formulated as $p' = (\sigma_1' + 2\sigma_c')/3$. Herein, the CSR value that causes $\varepsilon_{DA} = 5\%$ in 15 cycles (Nc) is defined as the liquefaction resistance of the soils and denoted as the cyclic resistance ratio, CRR; it is customary to consider $Nc = 15$ to be equivalent to 7.5 earthquake magnitude (Seed and Lee, 1966).

5. Cyclic yield strain concept

Amoly et al. (2016) proposed the concept of cyclic yield strain (ε_{ay}) that can mark a benchmark level of strain that allows not only to provide a boundary between liquefiable/non-liquefiable sands but also to estimate the yield point of soils during cyclic loading. Cyclic yield strain, ε_{ay}, is the ratio of the cyclic resistance ratio (at $\varepsilon_{DA} = 5\%$) to the small-strain shear modulus (G_{max}) of soils. Fig. 5 schematically depicts the procedures to estimate the ε_{ay} (Amoly et al., 2016):

- First, the liquefaction resistance curves of the materials are established for different double amplitude axial strains (ε_{DA}), see Fig. 5 (a). Then, using the developed liquefaction resistance curves, the CRR corresponding to 15 cycles are determined for different ε_{DA}, as shown by points A, B, C and D in Fig. 5 (a).
- Next, the obtained CRR values are plotted against their corresponding axial strain in Fig. 5 (b), i.e. points A, B, C and D. In this plot, the vertical axis represents the cyclic stress ratio (CSR) while the horizontal axis is expressed as single amplitude axial strain, i.e. $\varepsilon_{SA} = \varepsilon_{DA}/2$. The developed curve can be considered as a form of a non-linear stress-strain curve that is linked to the cyclic behaviour of soils. The graph depicts the change in liquefaction resistance with an increase in ε_{SA}. It

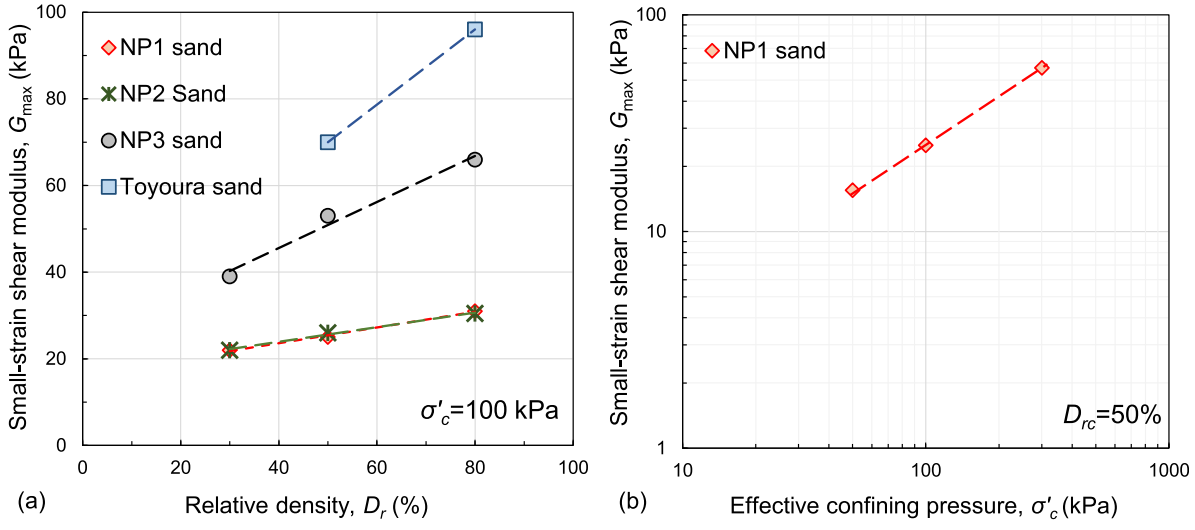

Fig. 4. Shear modulus dependency of reconstituted samples on (a) relative density; and (b) effective confining pressure.

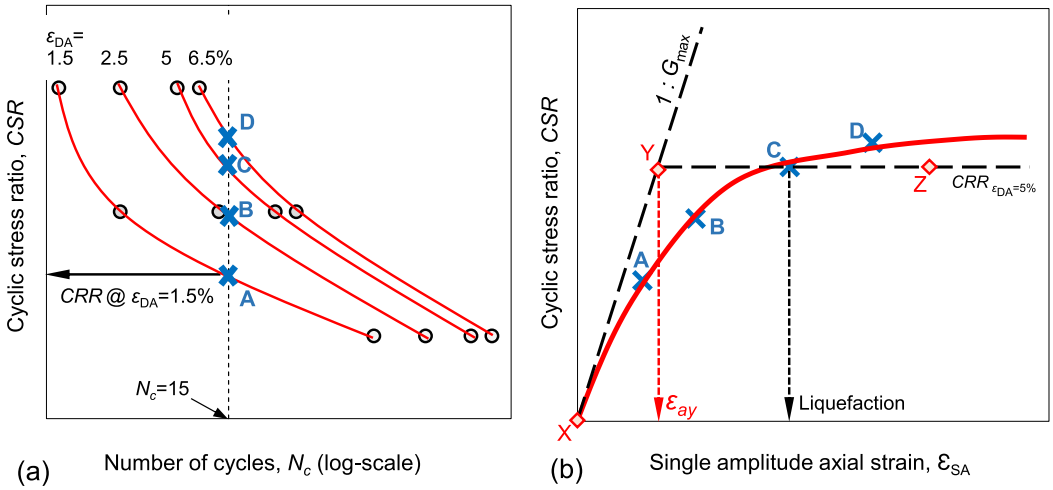

Fig. 5. Physical illustration of cyclic yield strain concept (modified from Amoly et al., 2016).

should be noted that, in this paper, the liquefaction resistance of NP sands was determined following normal engineering practice, i.e., based on double amplitude axial strain (ε_{DA}) criterion; however, in Amoly et al. (2016) approach, single amplitude axial strain ($\varepsilon_{DA}=\varepsilon_{SA}/2$) was used to represent typical stress-strain curves for cyclic yield strain determination. Therefore, ε_{SA} was also used here to develop the stress-strain plots, consistent with the approach presented in the literature.

- Then, the obtained non-linear stress-strain curve is presented by bi-linear lines: (1) the first tangent line is plotted from the origin with the slope equal to G_{max}; and (2) the second line is horizontal and crossed the *CRR* at $\varepsilon_{SA} = 2.5\%$ (i.e. $CRR@\ \varepsilon_{DA} = 5\%$); both lines are shown in Fig. 5 (b) as XY and YZ, respectively.
- As illustrated in Fig. 5 (b), the ε_{ay} is the level of strain that corresponds to the intersection of the bilinear lines (i.e., point Y). Therefore, the ε_{ay} is the ratio of *CRR* to the G_{max} of soils. According to Amoly et al. (2016), the *CSR* values in the vertical axis in Fig. 5 (b) are multiplied by the reference stress (P_a = 100 kPa) to make the value of ε_{ay} dimensionless, i.e., $\varepsilon_{ay} = (CRR \times P_a)/G_{max}$.

The higher magnitude of ε_{ay} represents a material with higher yield strain point during cyclic loading test (i.e., have flatter cyclic stress-strain curves) and vice versa. Amoly et al. (2016) speculated that the ε_{ay} is insensitive to the relative density (D_r) and only dependent on material type. This indicates the advantage of using ε_{ay} concept to estimate the yield strain point of soils during cyclic loading regardless of their degree of packing. Although Amoly et al. (2016) schematically indicate the independency of ε_{ay} on D_r, no data was presented to support their hypotheses, and the dependency of ε_{ay} on σ'_c was also not examined. Therefore, in this paper, the results from the reconstituted specimens are first used to illustrate the dependency of the ε_{ay} on D_r and σ'_c, as well as the applicability of the ε_{ay} concept for crushable volcanic soil.

6. Test results

6.1. Determination of ε_{ay}

The liquefaction resistance curves of NP sands at different levels of ε_{DA} (=1.5, 2.5, 5 and 6.5%) are illustrated in Fig. 6, while those for normal sands ($PC = 0\%$) are shown in Fig. 7; the results are for samples tested at $\sigma'_c = 100$ kPa. Fig. 6 exhibits the results for undisturbed samples from NP_{HMGS}, NP_{HMTR} and $NP_{TA,}$ as well as for the reconstituted NP1 results, while the results shown in Fig. 7 are for ordinary undisturbed NP_{TA7} sand and reconstituted Toyoura sand. The results for reconstituted samples are for post-consolidation relative density (Dr_c) of 50%. Each plot also depicts the G_{max} of the materials measured before the application of cyclic loading.

It can be seen from the graphs that the NP sands have different liquefaction resistance curves for different ε_{DA} values (i.e., the liquefaction resistance curves plot far from each other, see Fig. 6); whereas, the liquefaction resistance curves for normal sands show almost similar *CRR* over a wide range of ε_{DA} (see Fig. 7). The *CRR* - ε_{DA} relations for crushable NP sands and normal sands are compared in Fig. 8; note that the *CRR* values over different levels of ε_{DA} are normalised with respect to the *CRR* at $\varepsilon_{DA} = 5\%$. The developed *CRR* - ε_{DA} relations for all samples tested show generally linear relations within the range investigated. Furthermore, it is evident from Fig. 8 that the four types of NP sand (i.e., NP_{HMGS}, NP_{HMTR}, NP_{TA} and NP1) have a higher rate of increase in *CRR* when ε_{DA} increases, in contrast with non-pumiceous sands (i.e. NP_{TA7} and Toyoura sand), which show small changes in *CRR*. On the other hand, NP sands have considerably lower G_{max} values compared to ordinary sands (see the comparison in Fig. 6 and Fig. 7).

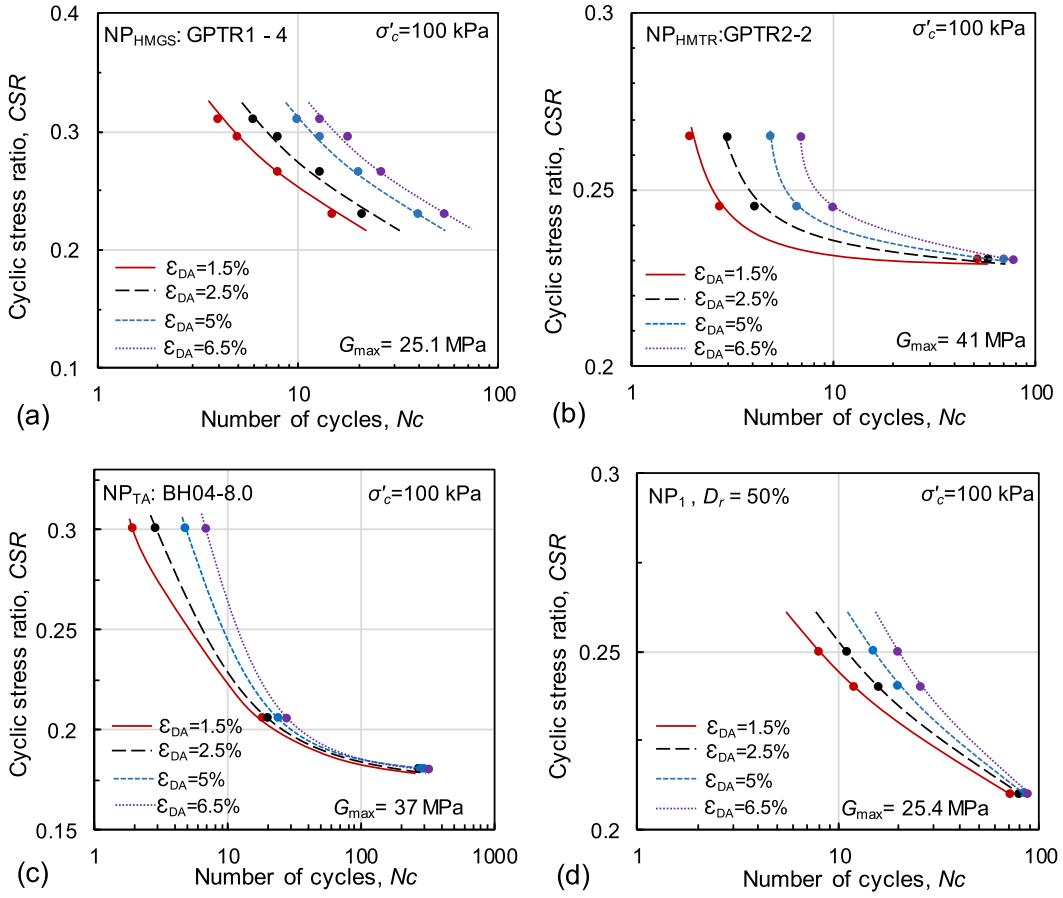

Fig. 6. Liquefaction resistance curves of NP sands for different ε_{DA} for undisturbed samples from (a) NP$_{HMGS}$; (b) NP$_{HMTR}$; (c) NP$_{TA}$; and reconstitited specimens from (d) NP1.

Next, following the procedure outlined by Amoly et al. (2016), the *CRR* of the materials are plotted with respect to their $\varepsilon_{SA} = \varepsilon_{DA}/2$ in Fig. 9 (a). Then, the bi-linear lines were drawn to represent the equivalent stress-strain relation of the samples to represent their cyclic behaviour. From the enlarged area shown in Fig. 9 (b), the values of cyclic yield strain (ε_{ay}) were estimated, representing the strain level at the intersections of the lines as shown by arrows. The obtained ranges of ε_{ay} for NP sands (i.e. 0.058% < ε_{ay} < 0.11%) are higher when compared with normal sands (i.e. $\varepsilon_{ay} \approx 0.023\%$).

6.2. Effect of confining pressure on ε_{ay}

To understand the effect of effective confining pressure on the liquefaction resistance of pumiceous sands as well

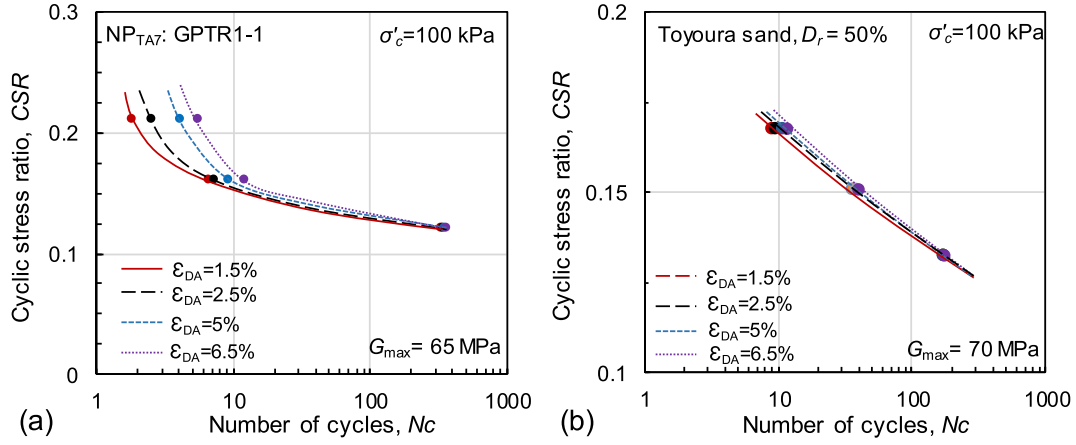

Fig. 7. Liquefaction resistance curves of normal sands ($PC = 0\%$) for different ε_{DA}: (a) undisturbed NP$_{TA7}$ sand; and (b) reconstituted Toyoura sand.

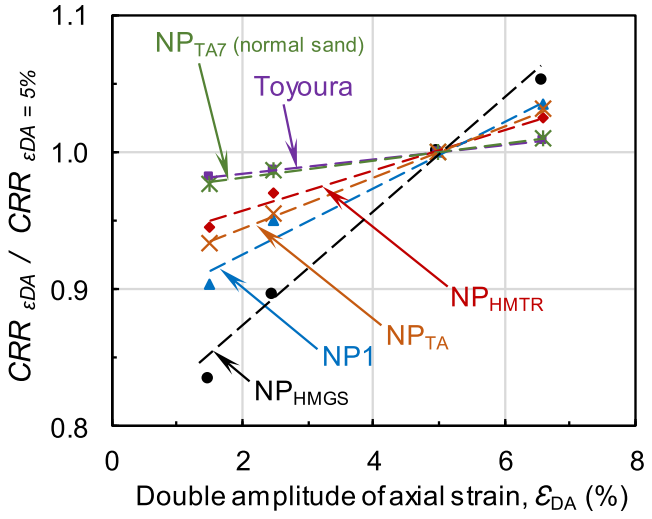

Fig. 8. Comparison of changes in cyclic resistance ratio with double amplitude axial strain.

as on their ε_{ay} value, cyclic triaxial tests were performed on reconstituted NP1 sand ($Dr_c \approx 50\%$) under variable levels of σ'_c (=50, 100 and 300 kPa). Fig. 9 (a) plots the cyclic shear stress ($q/2$) values required to reach $\varepsilon_{DA} = 5\%$ in 15 cycles versus the effective confining pressure of the samples. Since the ratio $q/2$ divided by σ'_c to attain $\varepsilon_{DA} = 5\%$ in $Nc = 15$ is defined as liquefaction resistance (CRR) of soils, the tangent lines in the plot have slopes equal to the CRR for different σ'_c.

It can be seen from Fig. 10 (a) that the magnitude of the cyclic shear stress (required for liquefaction to occur) increases with increasing σ'_c, whereas, their CRR decreases as σ'_c increases; this observation is consistent with the behaviour of normal sands (Idriss and Boulanger, 2008). Seed et al. (1983) introduced the overburden correction factor ($K_\sigma = CRR_{\sigma'c}/CRR_{\sigma'c=100\ kPa}$) to represent the dependency of the soil's liquefaction resistance to its effective confining pressure. The measured values of K_σ for NP1 sand are plotted versus their corresponding σ'_c and shown in Fig. 10 (b). It can be seen from the plot that NP1 sand, similar to the trend for normal sands, showed that the values of K_σ tend to decrease as σ'_c increases; however, NP1 sand showed a higher dependency of K_σ on σ'_c.

Regarding the cyclic yield strain (ε_{ay}) calculation proposed by Amoly et al. (2016), they used reference stress (i.e., $P_a = 100$ kPa) to multiply CRR values in order to non-dimensionalised the ε_{ay} ($=CRR \times P_a/G_{max}$) parameter, see vertical axis in Fig. 9. However, it was observed (from Fig. 10) that the CRR of soils has an indirect relation with σ'_c (i.e., $CRR \propto \frac{1}{\sigma'_c}$); hence, to have a better estimate of the level of cyclic shear stress applied to the samples, it is better to use the actual σ'_c rather than a constant P_a value. Moreover, the cyclic stress ratio (CSR) is defined as the ratio of cyclic shear stress ($q/2$) divided by σ'_c (i.e., $CSR = \frac{q}{2\sigma'_c}$). Consequently, using σ'_c to multiply the CSR values (in the vertical axis of Fig. 9) would provide the actual shear stress ($q/2$) applied to specimens; whereas, by using the reference stress (P_a), it is not possible to accurately represent the stress-strain plot related to their cyclic behaviour. Then, a modified version of cyclic yield strain (i.e., $\varepsilon_{ay,m}$) is proposed in the form

$$\varepsilon_{ay,m} = \frac{CRR \times \sigma'_c}{G_{max}} \quad (1)$$

To further elucidate the differences in using of P_a and σ'_c to develop the stress-strain relations, Fig. 11 (a) and (b) illustrate the established stress-strain relations using reference stress and the actual σ'_c, respectively. Note that the G_{max} used in Fig. 11 (a) is corrected for 100 kPa effective confining pressure while the utilised CRR is for the applied σ'_c (this is based on Amoly et al. (2016) approach). To correct the G_{max} values for the effect of confining pressure (for Fig. 11 (a)), the equation $G_{max1} = G_{max} \times (P_a/\sigma'_c)^m$, was used, where G_{max1} is the corrected G_{max} and m is the power coefficient expressing the effect of σ'_c. For the conversion, the m-value for NP1 sand sample was set at 0.72, as reported by Asadi et al. (2020). On the other hand, in Fig. 11 (b), the actual measured values of G_{max} and CRR at different σ'_c are used.

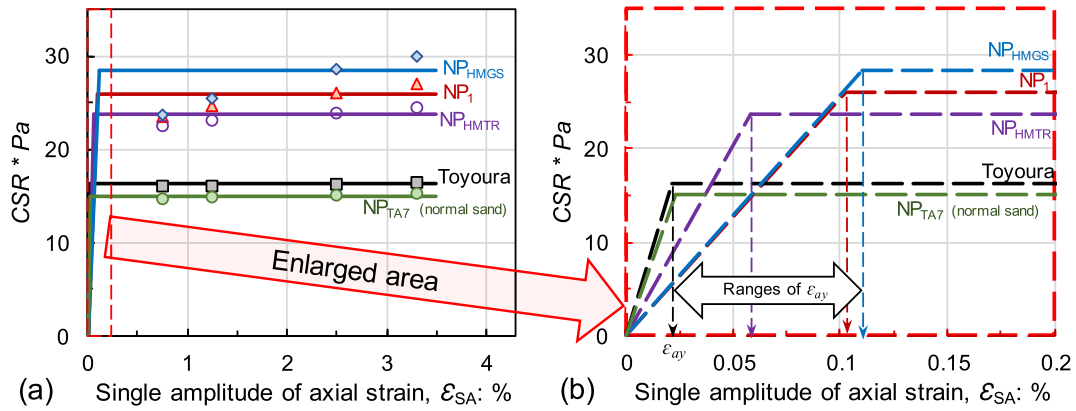

Fig. 9. (a) Development of the bi-linear stress-strain curves related to cyclic testing results; and (b) comparison of cyclic yield strains of different materials.

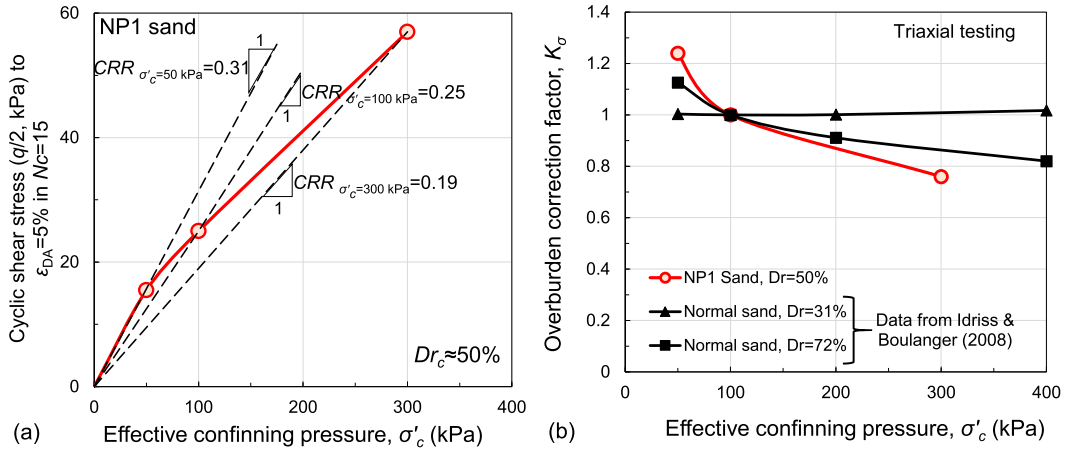

Fig. 10. Dependency of liquefaction resistance on effective confining pressure for NP1 sand: (a) $q/2 - \sigma'_c$ relation; and (b) overburden correction factor, K_σ.

It is evident from Fig. 11 (a) that using P_a resulted in an inaccurate estimation of shear stress subjected on the samples tested other than $\sigma'_c = 100$ kPa. i.e., Fig. 10 shows an increase in cyclic shear stress with increasing σ'_c; however, Fig. 11 (a) implied the opposite trend showing a decrease in shear stress with increases in σ'_c. On the other hand, using the actual applied σ'_c values to develop the stress-strain relations resulted in a demonstration of accurate levels of shear stress subjected to the samples during cyclic triaxial test. Furthermore, the cyclic yield strain values calculated with the σ'_c approach (see Fig. 11 b) leads to almost the same values of $\varepsilon_{ay,m}$ over a wide range of σ'_c. In contrast, Amoly et al. (2016) method (see Fig. 11 a) showed considerably different ε_{ay} values over wide ranges of σ'_c.

6.3. Effect of relative density on $\varepsilon_{ay,m}$

The effect of relative density (Dr_c) on $\varepsilon_{ay,m}$ was investigated for three types of NP sands (i.e. NP1, NP2 and NP3) as well as for Toyoura sand and the results are shown in Fig. 12. The NP specimens were prepared at three levels of Dr_c (≈30, 50 and 80%), while those of Toyoura sand were prepared at $Dr_c \approx 50$ and 80%; all samples were tested under $\sigma'_c = 100$ kPa. The results show an increase in the values of $CRR_{\varepsilon DA=5\%}$ and $G_{\max}$ with an increase in Dr_c for all sands tested. On the other hand, it is evident from the graphs that the estimated values of $\varepsilon_{ay,m}$ are less sensitive to the Dr_c of the samples (within the investigated ranges of Dr_c). For comparison purposes, the values of $\varepsilon_{ay,m}$ for different levels of Dr_c are plotted in Fig. 13 where it is seen that the $\varepsilon_{ay,m}$ is less sensitive to the specimen's degree of packing and highly dependent on the soil-type investigated. Therefore, $\varepsilon_{ay,m}$ can be used as an index parameter relating the yield strain point of sands during cyclic loading, regardless of their relative density. This is due to the fact that both CRR and $G_{\max}$ would increase with increase in Dr_c of the samples resulting in the bi-linear stress-strain curves (see Fig. 12) to have a similar level of yield strain. Indeed the rate of increase in CRR and $G_{\max}$ of the samples are different due to Dr_c variation; this is associated with small variation in the $\varepsilon_{ay,m}$ in relation with relative density, as shown in Fig. 13. The above investigation confirms the hypothesis made schematically by Amoly et al. (2016) that the cyclic yield strain is a

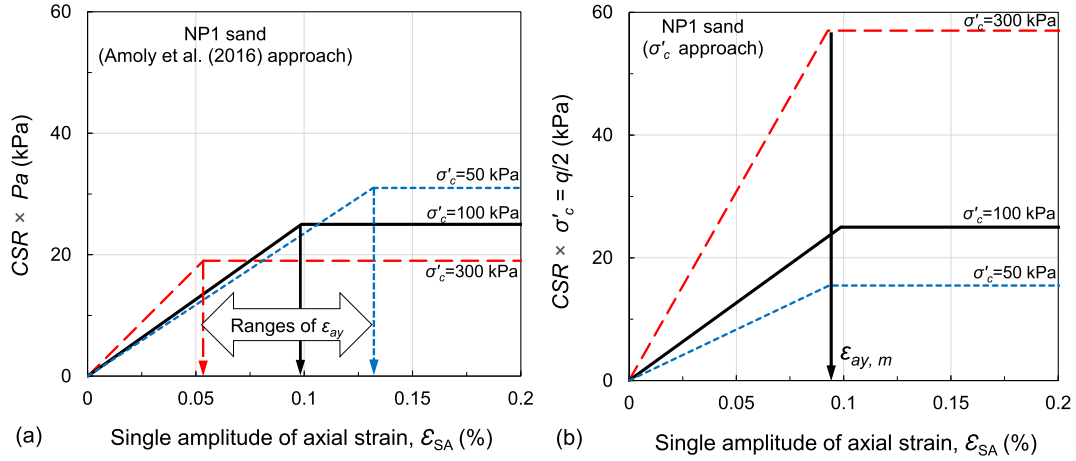

Fig. 11. Comparison of cyclic yield strain measurements using (a) reference stress, Amoly et al. (2016); and (b) effective confining pressure, this study.

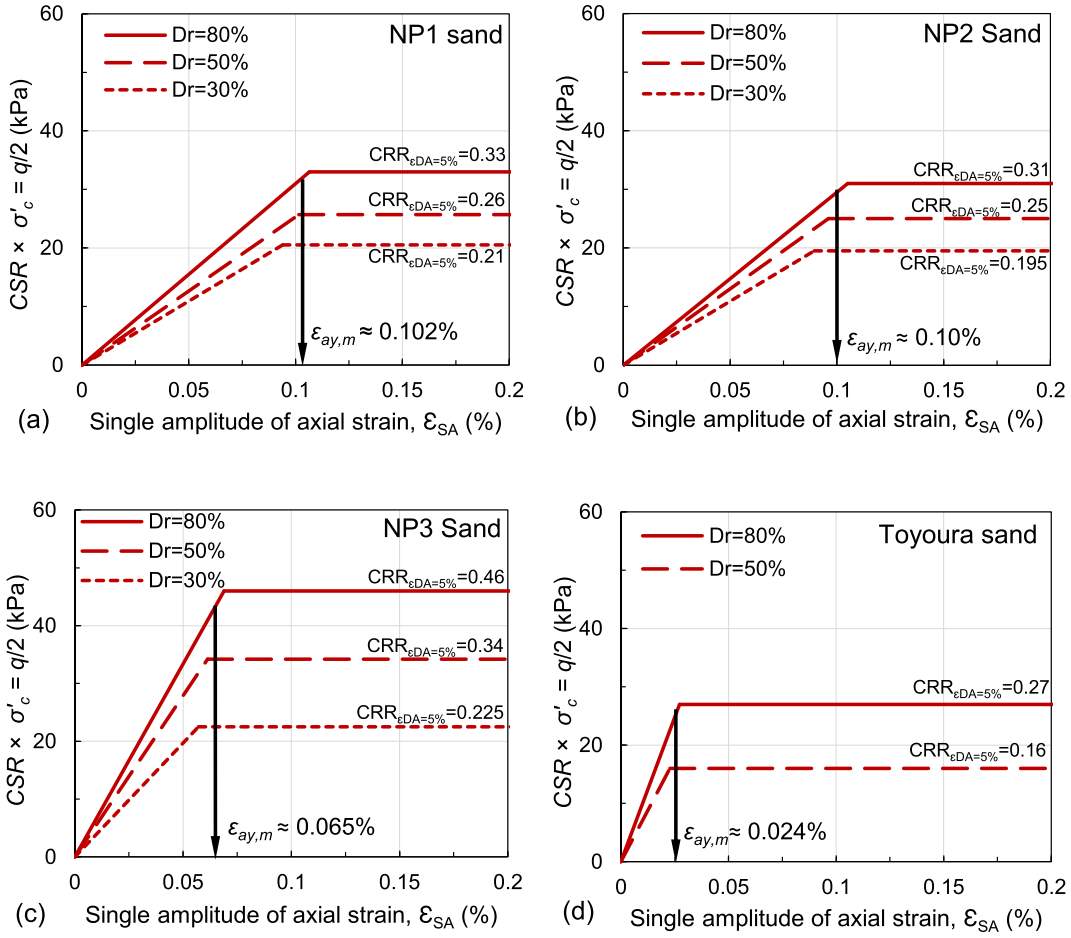

Fig. 12. Dependency of cyclic yield strain on relative density for reconstituted samples of (a) NP1 sand; (b) NP2 sand; (c) NP3 sand; and (d) Toyoura sand tested at $\sigma'_c = 100$ kPa.

material-dependent parameter and it would be less influenced by the material's degree of packing.

6.4. Effect of pumice content, fines content, and sample disturbance on $\varepsilon_{ay,m}$

The reconstituted/undisturbed NP sands collected from different sites have different pumice contents in their soil matrix (the estimated values of *PC* are shown in Table 1). Then, the obtained values of $\varepsilon_{ay,m}$ for NP sands are plotted against their estimated *PC* in Fig. 14. It is evident from the graph that the amplitude of $\varepsilon_{ay,m}$ is significantly influenced by the *PC* of the NP sands, i.e. as *PC* increases the $\varepsilon_{ay,m}$ value tends to increase. Furthermore, the results from Toyoura sand and ordinary NP_{TA7} sand as well as those of ordinary Japanese sands investigated by Amoly et al. (2016) are also illustrated in Fig. 14. Note that the results from Amoly et al. (2016) were obtained from both reconstituted and undisturbed specimens. It can be seen from the graph that the measured $\varepsilon_{ay,m}$ for NP sands at any level of *PC*, either reconstituted or undisturbed, showed higher $\varepsilon_{ay,m}$ when compared with those of normal sands. The higher $\varepsilon_{ay,m}$ of NP sands is because of the existence of angular and crushable pumice particles in their soil matrix, which would lead them to have higher *CRR* and lower G_{max} contributing to their higher cyclic yield strain with any level of *PC*.

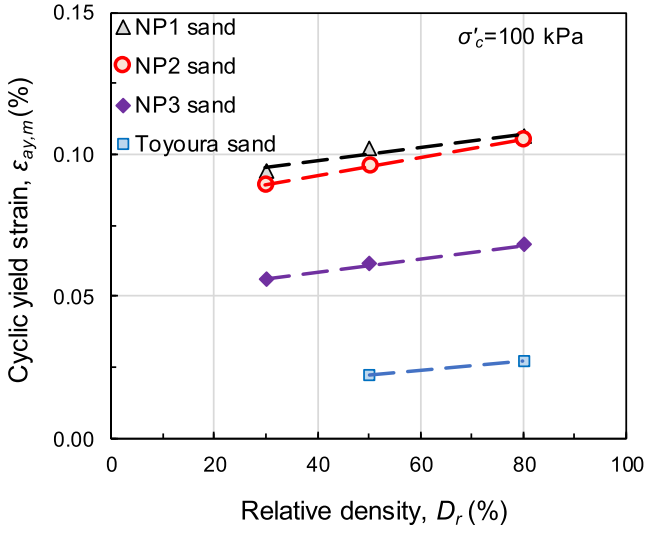

Fig. 13. Comparison of relative density effects on $\varepsilon_{ay,m}$ for different reconstituted samples.

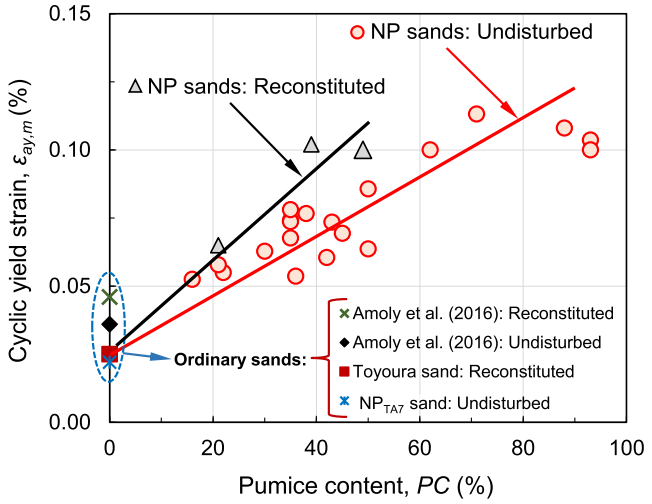

Fig. 14. Effects of pumice content on cyclic yield strain.

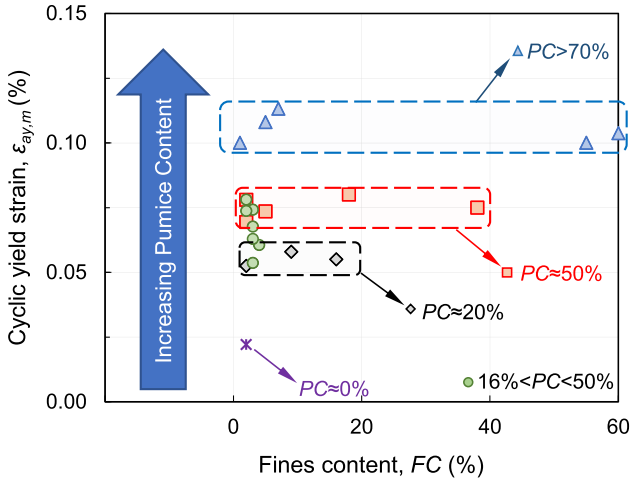

Fig. 15. Effects of fines content on cyclic yield strain.

Asadi et al. (2020) reported that NP sands experienced particle crushing after consolidation (under $\sigma'_c = 300$ kPa), while negligible crushing occurred in Toyoura sand. A similar observation was made by Asadi et al. (2018), who reported that pumice particles crushed during undrained cyclic loading, while almost none occurred in the case of Toyoura sand. Using the concept of relative breakage (B_r) index proposed by Hardin's (1985), Asadi et al. (2020) reported that with $\sigma'_c = 300$ kPa consolidation pressure, the B_r of NP1 sand (=0.058) and NP2 sand (=0.061) are almost twice of NP3 sand (=0.025) while Toyoura sand has $B_r = 0$; this shows the important effect of PC on the value of B_r.

It should be noted that most samples used in this study have low fines content ($FC < 10\%$) while only small numbers of them have high levels of FC (>30%). To understand the effect of FC on $\varepsilon_{ay,m}$ (from the limited number of samples have variable FC), the obtained values of $\varepsilon_{ay,m}$ are plotted versus their corresponding FC in Fig. 15. It is evident from the graph that the samples categorised as PC≈20%, PC≈50% and $PC > 70\%$ showed similar $\varepsilon_{ay,m}$, however, they have considerably different levels of fines content. Therefore, from the limited data presented herein, the effect of FC was found to be small on the $\varepsilon_{ay,m}$ values, in contrast with the effects of PC on the $\varepsilon_{ay,m}$. This can be explained using the investigations of Kayen et al. (2013) for the adjustment of $CRR - V_s$ relations for the effect of FC, i.e., they found minimal adjustment for the effect of FC on $CRR - Vs$ relations. Following Kayen et al. (2013) findings, similar tendency was also observed for the effect of FC on $\varepsilon_{ay,m}$, a relation between $CRR - G_{max}$, which is similar as $CRR - Vs$ relations. This is possibly due to the measurements of G_{max} and V_s at small strain level resulting to be less sensitive to the effect of fines content. To better understand the effect of FC, further studies are required/recommended to exclusively evaluate the effect of fines content on the $\varepsilon_{ay,m}$ value in the case of NP sands.

Moreover, Fig. 14 illustrates the differences between undisturbed and reconstituted specimens. The undisturbed samples showed slightly lower $\varepsilon_{ay,m}$ compared to those of reconstituted specimens with higher $\varepsilon_{ay,m}$. This observation can be attributed to the effects of soil fabric/age on the dynamic behaviour of sands. It is reasonable to speculate that the undisturbed specimens had a long history of soil deposition compared to those of reconstituted specimens. Therefore, undisturbed samples may have higher stiffness and higher liquefaction resistance resulting in their lower cyclic yield strain compared to those of reconstituted samples. This is also noted by Amoly et al. (2016) regarding the effect of soil fabric/age on the measured $\varepsilon_{ay,m}$ of the materials, who reported that the undisturbed specimens show lower cyclic yield strain.

7. Discussions

Natural pumiceous sands are a crushable material and have low G_{max} ($=\rho V_s^2$) compared to normal sands (Asadi et al. 2020). The crushability and low shear modulus of pumice particles lead NP sands to have flatter cyclic stress-strain plots while they have higher cyclic yield strain level. The undrained cyclic response of NP sands during the cyclic test is depicted in Fig. 16. The trends for NP sands illustrate the development of ε_{DA} from the beginning of cyclic loading application (Fig. 16 a), contributing to a sudden increase in excess pore water pressure ratio, r_u (Fig. 16 b); both ε_{DA} and r_u are plotted versus N_c normalised with respect to the N_c at $\varepsilon_{DA} = 5\%$. Normal sands, with higher G_{max} and negligible particle crushing, showed lower deformation in the first few N_c with significantly lower increases in r_u compared to NP sands. Note that the results for the undisturbed NP specimens in Fig. 16 are for specimens subjected to the same $CSR = 0.25$, while they were sourced from different sites. On the other hand, the results for reconstituted NP sands and Toyoura sand were for those reconstituted at $Dr_c = 50$ and 80%. Since the reconstituted specimens had quite different CRR, it

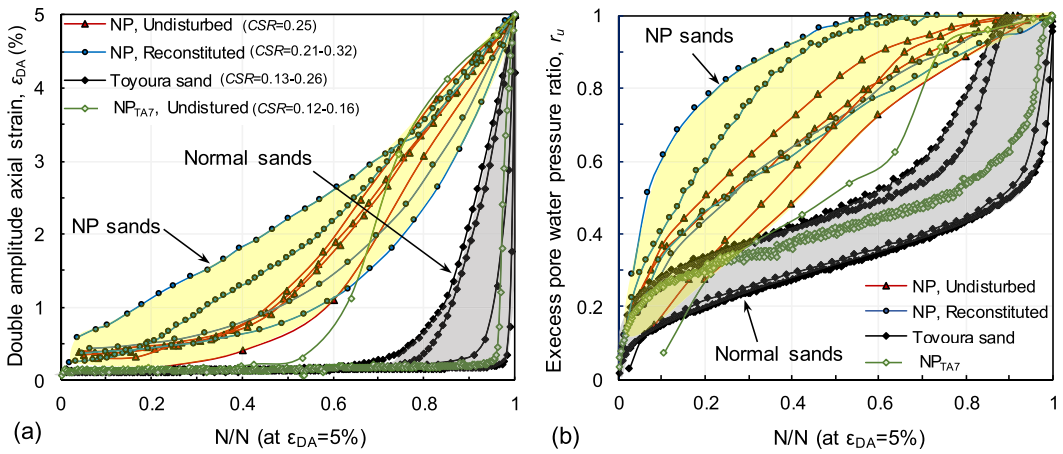

Fig. 16. Comparison of development of (a) double amplitude axial strain, ε_{da}; and (b) excess pore water pressure ratio, r_u against normalised number of cycles for the materials tested.

was not possible to compare their cyclic behaviour under the same *CSR*, and the ranges of *CSR* applied are shown in Fig. 16. Therefore, the NP specimens tested with different soil properties, Dr_c and soil fabric/age showed generally similar cyclic behaviour, which is significantly different compared to normal sands. In addition, the observed cyclic response of Toyoura sand and ordinary NP_{TA7} sand is consistent with the observation on other normal sands (Idriss and Boulanger 2008; Ishihara 1993; Taylor 2014; Toki et al., 1986).

NP sands show higher deformability during the initial stages of cyclic loading; however, towards the end of the test, they can be subjected to further cycles with gradual deformation until the occurrence of liquefaction, hence, they have higher yield strain point and higher *CRR* values (Asadi et al., 2018). The above contradictory observation during different stages of cyclic test can be explained using the discrete element method (DEM) studies on granular sands. The DEM investigations emphasised that G_{max} and *CRR* of granular soils (under identical D_r and σ'_c) are independently governed by two different micro-parameters: (1) shear modulus (related to deformability); and (2) inter-particle friction (related to *CRR*), respectively (Chang et al., 1991; Santamarina and Cascante, 1996; Xu et al., 2015; Yimsiri and Soga, 2000). Following the DEM studies, during the initial stages of cyclic loading, the low G_{max} and crushability of NP sands causes the soil assembly to be more deformable, resulting in a faster increase in particle contacts in the soil sample. Due to the higher increase in particle contacts between the irregular-shaped pumice particles within the soil matrix, better soil particle interlocking is manifested toward the end of the test, leading to their higher *CRR*. Furthermore, Fig. 8 shows the above restructuration happens for NP sands during cyclic test resulting in better improvement in *CRR* as the level of ε_{DA} increases, on the other hand, normal sands show small increases in *CRR* with increasing ε_{DA}.

The relation between *CRR* (at $\varepsilon_{DA} = 5\%$) and G_{max} of the undisturbed and reconstituted materials are illustrated in Fig. 17 (a) and (b), respectively. It can be seen from the graphs that the NP sands with different *PC* have significantly different *CRR* - G_{max} relations. Furthermore, NP sands have substantially different *CRR* - G_{max} relations when compared with the normal sands. For example, the undisturbed/reconstituted NP samples with higher *PC* values indicated a higher CRR/G_{max} ratio and this ratio tends to decrease for the samples categorised as low *PC* materials. Furthermore, the CRR/G_{max} ratio for ordinary sands showed considerably lower values compared with NP sands. These results indicate that the CRR/G_{max} ratio can distinguish NP sands with different *PC* and with those of normal sands. In a soil assembly consisting of normal sand and pumice sand, the voids that form between the soil grains would increase with an increase in the number of porous and angular pumice components. This is due to the contact of irregular pumice particles with other constituents at their jagged contact points; the angularity of NP samples is shown in Fig. 18, which taken from undisturbed low *PC* and high *PC* samples. Then, the specimens with a higher level of *PC* would have a higher level of void ratios (under the same *Dr*) and higher crushability potential, leading to their greater deformability (have lower G_{max}). Due to cyclic loading application, the high *PC* samples with a greater number of irregular-shaped pumice particles provide good interlocking and/or re-structuring in soil assembly, resulting in higher *CRR* (better improvements in the *CRR* of NP sands with increasing ε_{DA} can be seen in Fig. 8 for the specimens with higher *PC*).

According to the above observations, the shear modulus and angularity of soil particle would independently have important influences on the cyclic behaviour of granular soils. Using cyclic yield strain parameter ($\varepsilon_{ay,m} \propto CRR/G_{max}$) would allow consideration of the significant effects of both shear modulus and irregular shape of soil particles on the cyclic behaviour of soils in the form of a single

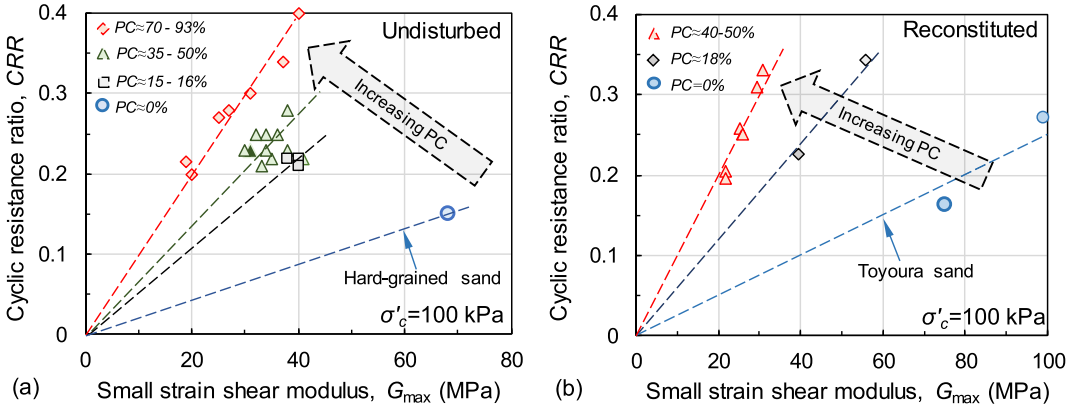

Fig. 17. The relation of *CRR* with G_{max} of NP sands having different pumice content for those of (a) undisturbed; and (b) reconstituted samples.

parameter. Furthermore, $\varepsilon_{ay,m}$ was found to be a material-type parameter and was less sensitive to the specimen's degree of packing and effective confining pressure, in contrast to *CRR* and G_{max} that are both highly dependent on the specimen's *Dr* and σ'_c. These findings emphasise the advantages of using the $\varepsilon_{ay,m}$ approach to analysis the undrained cyclic response of crushable volcanic sands. Because NP sands have substantially higher *CRR* values in relation to their low shear modulus (and rapid r_u development from the beginning of cyclic loading); this could lead to misinterpretation of their liquefaction resistance. Thus, the $\varepsilon_{ay,m}$ approach can highlight their higher yield strain characteristics (i.e., low G_{max} and high *CRR*). Fig. 14 indicated that the NP sands have considerably higher $\varepsilon_{ay,m}$ (=0.055–0.12%) values depending on their *PC*, contrasting them from normal sands with low $\varepsilon_{ay,m}$ (=0.024–0.046%). Consequently, as $\varepsilon_{ay,m}$ relates *CRR* to G_{max} ($=\rho V_s^2$), and it is a material-dependent parameter, and having low sensitivity to relative density and confining pressure, $\varepsilon_{ay,m}$ can be used as a constant strain parameter to establish empirical *CRR*-V_s relations for possible use in estimating the liquefaction resistance of NP sands while considering their pumice contents. To sum up, $\varepsilon_{ay,m}$ is highly dependent on the *PC* of NP sands and, therefore, different values of $\varepsilon_{ay,m}$ can be utilised depending on the *PC* of the material to develop *CRR*-V_s relations for estimating the liquefaction resistance of NP sands (Asadi et al., 2021).

It should be mentioned that the findings presented here were for NP sands obtained in the Taupo Volcanic Zone, and therefore may be limited to certain composition, mineralogy, and other characteristics of the pumice source. Nevertheless, it is believed that the concept can be used as a tool to examine the liquefaction characteristics of volcanic sands available in other parts of the world, especially those containing crushable pumice sands.

8. Conclusions

Several series of undrained cyclic triaxial and bender element tests were performed on undisturbed and reconstituted natural pumiceous (NP) specimens to measure their cyclic resistance ratio (*CRR*) and small-strain shear modulus (G_{max}). Furthermore, the modified cyclic yield strains

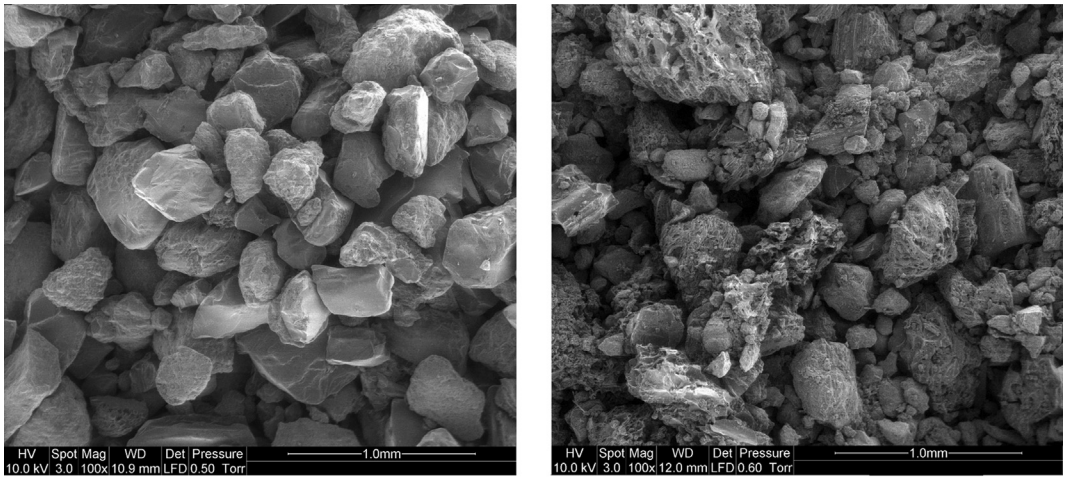

Fig. 18. SEM images of undisturbed samples obtained from NP_{WH} site categorised as (a) low *PC* sample; and (b) high *PC* sample.

($\varepsilon_{ay,m}$) were estimated using the *CRR* and G_{max} results obtained from NP sands. For comparison purposes, similar tests were also performed on specimens of normal ($PC = 0\%$) sands. The major conclusions of this study are as follows:

The presence of crushable and porous pumice components in the natural pumiceous sands resulted in their lower G_{max}. It follows the higher deformability of NP sands during cyclic test contributed to a substantial increase in pore water pressure during cyclic loading.

The occurrence of pumice particle crushing resulted in significant increases in particle-to-particle contacts, subsequently, the irregularly-shaped pumice particles provided a good interlocking between NP sand particles, leading to their higher *CRR*.

The cyclic yield strain ($\varepsilon_{ay,m}$) parameter, relating *CRR* and G_{max}, was found to be less sensitive of the effective consolidation stress and relative density within the investigated range of the tested samples. However, $\varepsilon_{ay,m}$ was found to be significantly dependent on the material-type and the pumice content of the NP sands.

NP sands have substantially higher values of $\varepsilon_{ay,m}$ ($\approx 0.055\%-0.12\%$), indicating their higher *CRR* as well as lower G_{max}, when compared to those of normal sands with lower $\varepsilon_{ay,m} \approx 0.022\%-0.024\%$. Furthermore, NP sands with a higher level of pumice content showed higher $\varepsilon_{ay,m}$ values than those with lower *PC*. This would indicate the significant effect of pumice components on the dynamic properties of NP sands.

The $\varepsilon_{ay,m}$ parameter can better represent the cyclic response of NP sands with quite high *CRR* relative to their very low G_{max}. For instance, the high values of $\varepsilon_{ay,m}$ would clearly indicate the low stiffness (high deformability) of NP sands due to their low G_{max}. Furthermore, the high values of $\varepsilon_{ay,m}$ would also show that the NP sands have stronger resistance against liquefaction (i.e., higher *CRR*).

Acknowledgements

The authors would like to acknowledge the advice of Professor Kenji Ishihara of Tokyo University of Science, Japan, in the development of this study. Furthermore, the assistance of Dr Mark Stringer, Tonkin and Taylor Ltd., AECOM, and WSP in facilitating access to the site and in providing some samples and site details is gratefully acknowledged. The permission to do field testing from Whakatane District Council and Hamilton City Council is gratefully acknowledged. The first author also gratefully acknowledged the PhD scholarship supports from the Natural Hazards Research Platform (NHRP) and QuakeCoRE, a New Zealand Tertiary Education Commission-funded Centre. This is QuakeCoRE Publication Number 0724.

References

Abdoun, T., Gonzalez, M.A., Thevanayagam, S., Dobry, R., Elgamal, A., Zeghal, M., Mercado, V.M., El Shamy, U., 2013. Centrifuge and large-scale modeling of seismic pore pressures in sands: cyclic strain interpretation. J. Geotech. Geoenviron. Eng. 139 (8), 1215–1234.

Amoly, R.S., Ishihara, K., Bilsel, H., 2016. The relation between liquefaction resistance and shear wave velocity for new and old deposits. Soils Found. 56 (3), 506–519.

Andrus, R.D., Stokoe II, K.H., 2000. Liquefaction resistance of soils from shear-wave velocity. J. Geotech. Geoenviron. Eng. 126 (11), 1015–1025.

Asadi, M.B., Asadi, M.S., Orense, R.P., Pender, M.J., 2020. Small-strain stiffness of natural pumiceous sand. J. Geotech. Geoenvirom. Eng. 146 (6), 06020006.

Asadi, M.B., Orense, R.P., Asadi, M.S., Pender, M.J., 2021. "Empirical assessment of liquefaction resistance of crushable pumiceous sand using shear wave velocity. J. Geotech. Geoenviron. Eng., under review

Asadi, M.S., Asadi, M.B., Orense, R.P., Pender, M.J., 2018. Undrained cyclic behavior of reconstituted natural pumiceous sands. J. Geotech. Geoenviron. Eng. 144 (8), 04018045.

Asadi, M.S., Orense, R.P., Asadi, M.B., Pender, M.J., 2019. Maximum dry density test to quantify pumice content in natural soils. Soils Found. 59 (2), 532–543.

Beanland, S., Berryman, K.R., Blick, G.H., 1989. Geological investigations of the 1987 Edgecumbe earthquake, New Zealand. N. Z. J. Geol. Geophys. 32 (1), 73–91.

Chang, C.S., Misra, A., Sundaram, S.S., 1991. Properties of granular packings under low amplitude cyclic loading. Soil Dyn. Earthquake Eng. 10 (4), 201–211.

Crenairz (2010). "Soil liquefaction." EERI Chile Earthquake Clearinghouse, http://www.eqclearinghouse.org/.

de Cristofaro, M., Olivares, L., Orense, R.P., Asadi, M.S., Netti, N., 2022. Liquefaction of volcanic soils: undrained behavior under monotonic and cyclic loading. J. Geotech. Geoenviron. Eng. 148 (1), 04021176.

Dobry, R., 1989. Some basic aspects of soil liquefaction during earthquakes. Ann. N. Y. Acad. Sci. 558 (1), 172–182.

Dobry, R., Abdoun, T., Stokoe, K.H., Moss, R.E.S., Hatton, M., El Ganainy, H., 2015. Liquefaction potential of recent fills versus natural sands located in high-seismicity regions using shear-wave velocity. J. Geotech. Geoenviron. Eng. 141 (3), 04014112.

Dobry, R., Ladd, R.S., Yokel, F.Y., Chung, R.M., Powell, D., 1982. Prediction of pore water pressure buildup and liquefaction of sands during earthquakes by the cyclic strain method. NBS Building Science Series 138, National Bureau of Standards.

Gratchev, I., Towhata, I., 2010. Geotechnical characteristics of volcanic soil from seismically induced Aratozawa landslide, Japan. Landslides 7 (4), 503–510.

Hardin, B.O., 1985. Crushing of soil particles. J. Geotechn. Eng., ASCE 111 (10), 1177–1192.

Hazarika, H., Kokusho, T., Kayen, R.E., Dashti, S., Fukuoka, H., Ishizawa, T., Kochi, Y., Matsumoto, D., Furuichi, H., Hirose, T., Fujishiro, T., Okamoto, K., Tajiri, M., Fukuda, M., 2017. Geotechnical damage due to the 2016 Kumamoto earthquake and future challenges. Lowland Technol. Int. 19 (3), 189–204.

Hsu, C.-C., Vucetic, M., 2004. Volumetric threshold shear strain for cyclic settlement. J. Geotech. Geoenviron. Eng. 130 (1), 58–70.

Hyodo, M., Hyde, A.F.L., Aramaki, N., 1998. Liquefaction of crushable soils. Geotechnique 48 (4), 527–543.

Idriss, I.M., Boulanger, R.W., 2008. Soil Liquefaction during Earthquakes, Oakland, Calif. Earthquake Engineering Research Institute.

Ishihara, K., 1993. Liquefaction and flow failure during earthquakes. Geotechnique 43 (3), 351–451.

Ishihara, K., Harada, K., 1994. Cyclic behavior of partially saturated collapsible soils subjected to water permeation. Geotechnical Special Publication 44, 34–50.

Japanese Geotechnical Society, JGS, 2000. Soil Test Procedure and Commentaries, Revised 1st Ed., Tokyo (in Japanese).

Kayen, R., Moss, R.E.S., Thompson, E.M., Seed, R.B., Cetin, K.O., Kiureghian, A.D., Tanaka, Y., Tokimatsu, K., 2013. Shear-wave velocity-based probabilistic and deterministic assessment of seismic soil liquefaction potential. J. Geotech. Geoenviron. Eng. 139 (3), 407–419.

Kazama, M., Kataoka, S., Uzuoka, R., 2012. Volcanic mountain area disaster caused by the Iwate-Miyagi Nairiku Earthquake of 2008, Japan. Soils Found. 52 (1), 168–184.

Kikkawa, N., Orense, R.P., Pender, M.J., 2013. Observations on microstructure of pumice particles using computed tomography. Can. Geotech. J. 50 (11), 1109–1117.

Kokusho, T., Hazarika, H., Ishizawa, T., 2019. Geotechnical damage by liquefaction-induced failure during 2018 Hokkaido Iburi-East earthquake. Proceedings of the 7th International Conference on Earthquake Geotechnical Engineering, Rome, Italy.

Ladd, R.S., Dobry, R., Dutko, P., Yokel, F.Y., Chung, R.M., 1989. Pore-water pressure buildup in clean sands because of cyclic straining. Geotech. Test. J. 12 (1), 77.

Marks, S., Larkin, T.J., Pender, M.J., 1998. The dynamic properties of a pumiceous sand. Bull. New Zealand National Society Earthquake Eng. 31 (2), 86–102.

McCraw, J., 2011. The wandering river: Landforms and geological history of the Hamilton Basin. Geoscience Society of New Zealand Guidebook.

Ministry of Transport Japan, 1999. Technical Standards and Commentaries for Port and Harbour in Japan. The Overseas Coastal Area Development Institute of Japan.

Miura, S., Yagi, K., Asonuma, T., 2003. Deformation-strength evaluation of crushable volcanic soils by laboratory and in-situ testing. Soils Found. 43 (4), 47–57.

Orense, R.P., Pender, M.J., O'Sullivan, A., 2012. Liquefaction characteristics of pumice sands. Report No. EQC 10/589. Auckland, New Zealand: University of Auckland.

Papa, R., Evangelista, A., Nicotera, M.V., Urciuoli, G., 2008. Mechanical properties of unsaturated pyroclastic soils affected by fast landslide phenomena. Proceedings of the 1st European Conference on Unsaturated Soils, E-UNSAT 2008, pp. 917-923.

Pender, M.J., Robertson, T.W., 1987. Edgecumbe earthquake: reconnaissance report. Bull. New Zealand National Soc. Earthq. Eng. 20 (3), 201–249.

Picarelli, L., Evangelista, A., Rolandi, G., Paone, A., Nicotera, M.V., Olivares, L., Scotto Di Santolo, A., Lampitiello, S.,Rolandi, M., 2007. Mechanical properties of pyroclastic soils in Campania Region. Proceedings of the Characterisation and Engineering Properties of Natural Soils, Taylor & Francis, 2331-2383.

Sahaphol, T., Miura, S., 2005. Shear moduli of volcanic soils. Soil Dyn. Earthquake Eng. 25 (2), 157–165.

Sandoval, E.A., Pando, M.A., 2012. Experimental assessment of the liquefaction resistance of calcareous biogenous sands. Earth Sci. Res. J. 16 (1), 55–63.

Santamarina, J.C., Cascante, G., 1996. Stress anisotropy and wave propagation: a micromechanical view. Can. Geotech. J. 33 (5), 770–782.

Seed, H.B., Idriss, I.M., Arango, I., 1983. Evaluation of liquefaction potential using field performance data. J. Geotech. Eng. 109 (3), 458–482.

Seed, H.B., Lee, K.L., 1966. Liquefaction of saturated sands during cyclic loading. J. Soil Mech. Foundation Division 92 (6), 105–134.

Shirley, D.J., Hampton, L.D., 1978. Shear-wave measurements in laboratory sediments. J. Acoust. Soc. Am. 63 (2), 607–613.

Standards New Zealand, 1986. NZS4402, Test 4.2.2. Methods of testing soils for civil engineering purposes. Wellington, New Zealand.

Stringer, M., Taylor, M., Cubrinovski, M., 2015. Advanced soil sampling of silty sands in Christchurch. Report No: 2015-06. University of Canterbury, New Zealand.

Suzuki, M., Yamamoto, T., 2004. Liquefaction characteristic of undisturbed volcanic soils in cyclic triaxial test. Proceedings of the 13th World Conference on Earthquake Engineering, Vancouver, B.C., Canada, Paper No. 465.

Taylor, M.L., 2014. The geotechnical characterisation of Christchurch sands for advance soil modelling. PhD Thesis, University of Canterbury, New Zealand.

Toki, S., Tatsuoka, F., Miura, S., Yoshimi, Y., Yasuda, S., Makihara, Y., 1986. Cyclic undrained triaxial strength of sand by a cooperative test program. Soils Found. 26 (3), 117–128.

Verdugo, R., Ishihara, K., 1996. The steady state of sandy soils. Soils Found. 36 (2), 81–91.

Xu, X.M., Ling, D.S., Cheng, Y.P., Chen, Y.M., 2015. Correlation between liquefaction resistance and shear wave velocity of granular soils: a micromechanical perspective, *Proc*. Geotech. Earthquake Eng. - Geotechnique Symposium in Print 2015, 13–24.

Yang, J., Gu, X.Q., 2013. Shear stiffness of granular material at small strains: does it depend on grain size? Geotechnique 63 (2), 165–179.

Yimsiri, S., Soga, K., 2000. Micromechanics-based stress-strain behaviour of soils at small strains. Geotechnique 50 (5), 559–571.